Atomic-scale structure of the glassy Ge 2 Sb 2 Te 5 phase change material: A quantitative assessment via first-principles molecular dynamics

Assil Bouzid, Guido Ori, Mauro Boero, Evelyne Lampin, Carlo Massobrio

Atomic-scale structure of the glassy $Ge_2Sb_2Te_5$ phase change material: A quantitative assessment via first-principles molecular dynamics

Assil Bouzid,[1,*] Guido Ori,[1] Mauro Boero,[1] Evelyne Lampin,[2] and Carlo Massobrio[1]
[1]*Université de Strasbourg, CNRS, Institut de Physique et Chimie des Matériaux de Strasbourg, UMR 7504, F-67034 Strasbourg, France*
[2]*Université de Lille, CNRS, Centrale Lille, ISEN, Université Valenciennes, UMR 8520 - IEMN, F-59000 Lille, France*

The amorphous structure of the phase change material $Ge_2Sb_2Te_5$ (GST) has been the object of controversial structural models. By employing first-principles molecular dynamics within density functional theory, we are able to obtain quantitative agreement with experimental structural findings for the topology of glassy GST. To this end, we take full advantage of a thoughtful, well established choice of the exchange-correlation (XC) functional (Becke-Lee-Yang-Parr, BLYP), combined with appropriate options for the nonlocal part in the pseudopotential construction for Ge. Results obtained by using the Perdew-Burke-Ernzerhof (PBE) XC functional and a similar strategy for the Ge pseudopotential constructions are also presented, since they are very valuable and worthy of consideration. The atomic structure of glassy GST is characterized by Ge atoms lying in a predominant tetrahedral network, albeit a non-negligible fraction of Ge atoms are also found in defective octahedra.

I. INTRODUCTION

$Ge_2Sb_2Te_5$ (GST hereafter) is the most established and successful phase change material (PCM) [1,2] due to its high switching speed and its remarkable optical contrast between the amorphous and the crystalline phases. To exploit the properties of GST and optimize applications, a precise understanding of its atomic scale network and bonding properties is highly desirable. This can be highly beneficial to unveil the cause of current technological limitations involving resistance drift and threshold switching phenomena [3,4]. Despite the known dependence of the local order of amorphous GST on the sample processing [5,6], the structure of the GST network (mostly octahedral, tetrahedral, or containing both) and its bonding nature remain elusive [7,8]. Experimentally, x-ray absorption fine structure (EXAFS) and x-ray absorption near-edge structure (XANES) measurements [9] point toward predominant tetrahedral Ge motifs, in contrast to the octahedral arrangement of the crystalline phase. Further refinement by EXAFS and bond constraint theory [10,12] revealed a high concentration of Ge–Ge homopolar bonds, along with overcoordinated Te sites. However, ^{125}Te nuclear magnetic resonance (NMR) spectroscopy [13] proposed a mixed Te coordination environment that consists solely of heteropolar Ge/Sb-Te bonds. Also, x-ray fluorescence holography performed on an epitaxial GST layer highlighted the occurrence of a cubic structure with a tetrahedral symmetry around Ge sites [14]. The displacements of Ge atoms from octahedral to tetrahedral sites was found at the very origin of a nonthermal crystal-to-amorphous phase transition via ultrafast time-resolved electron diffraction experiments [15].

The question arises on the capability of a modeling scheme based on density functional theory (DFT) to elucidate the atomic structure of GST in a way consistent with experiments. We are referring here to the structural optimization or evolution of temporal trajectories at finite temperatures, as performed within first-principles molecular dynamics (FPMD). While the amorphous state [16] was first rationalized in terms of a spinal-like geometry (tetrahedral geometry), subsequent FPMD simulations revealed the coexistence of tetrahedral and octahedral Ge sites [17–19], in puzzling contrast with EXAFS data. Overall, it appears that FPMD approaches have been instrumental to unravel the fundamental features of several processes inherent in the behavior of GST (as the crystallization mechanism, for instance). However, available FPMD models overestimate Ge–Ge, Ge–Te, and Sb–Te bond lengths obtained by EXAFS measurements leading to not entirely satisfactory predictions for neutron structure factors and pair correlation functions [17–21].

This observation prompts the search of alternative approaches to describe glassy GST at the atomic scale. Such motivation is substantiated by recent achievements obtained for glassy $GeTe_4$ [22] using the Becke-Lee-Yang-Parr [23,24] (BLYP) exchange-correlation (XC) functional and appropriate pseudopotentials (PPs) [25].

In this paper, we exploit the modeling framework of Ref. [22] to carry out FPMD calculations of glassy $Ge_2Sb_2Te_5$. Our results are in very good agreement with x-ray [9,10], neutron scattering [26,27], and EXAFS [10,14,28] measurements, as shown by comparison with published FPMD data.

The present paper is organized as follows. In Sec. II, we provide details of our calculation methodology, built on the use of two different XC functionals and well calibrated choices for the PPs and their construction. Section III is devoted to our results and it is organized in subsections. The first features the comparison between theory and experiments for the total structure factor $S(k)$, followed by the analysis of the total and partial pair correlation function $g(r)$. Then, we move to the coordination numbers. In a final section, we highlight correlations between structural and electronic properties by relying on the Wannier functions formalism. Conclusions are contained in Sec. IV.

*Present address: Chaire de Simulation à l'Echelle Atomique (CSEA), Ecole Polytechnique Fédérale de Lausanne (EPFL), CH-1015 Lausanne, Switzerland.

II. METHODOLOGY OF CALCULATIONS

We adopted the Car-Parrinello [29] approach (CPMD) [30] by making use of the BLYP XC functional or the Perdew-Burke-Ernzerhof (PBE) XC functional [31]. The valence-core interaction is described by either norm-conserving Troullier-Martins (TM) PPs (PBE-TM and BLYP-TM) or by norm-conserving Goedecker, Teter and Hutter (GTH) PPs [32,33] (BLYP-GTH). Valence electrons are represented by a plane-wave basis set expanded at the Γ point of the simulation cell with an energy cutoff of 30 Ry. A fictitious electron mass of 500 a.u. and a time step $\Delta t = 0.12$ fs ensured optimal conservation of the constant of motion. The ionic temperature was controlled with a Nosé-Hoover [34–36] thermostat chain [37], whereas for the fictitious electronic kinetic energy we used a Blöchl-Parrinello thermostat [38] with the target kinetic energy set to 0.04 au. We adopted the Kleinman-Bylander (KB) construction [39] based on a local component $V^{\rm loc}(\mathbf{r})$ and a pseudoatomic eigenstate $|\phi_{l,m}\rangle$ expansion for the nonlocal term. We remind that the Kleinman-Baylander construction of PPs is based on a separable form where we distinguish between a local and a nonlocal part:

$$V_{\rm KB} = V_{\rm loc}(r) + \sum_{lm}^{l^{\rm max}} \frac{|V_l'(r)\phi_{lm}\rangle\langle V_l'(r)\phi_{lm}|}{\langle\phi_{lm}|V_l'(r)|\phi_{lm}\rangle}, \qquad (1)$$

where $V_{\rm loc}(r)$ is the local part of the potential, $V_l'(r) = V_{\rm PS}(r) - V_{\rm loc}(r)$ is the nonlocal part of the potential, and $V_{\rm PS}(r)$ is the atomic potential of the reference state. ϕ_{lm} denotes the eigenstate of the atomic pseudo-Hamiltonian. While the choice of the local part $V_{\rm loc}(r)$ is arbitrary, one typically truncates the sum over the angular momentum lm at a given value $l^{\rm max}$. BLYP-GTH PPs were found insensitive to the KB construction choice. In the case of TM PPs, for both Sb and Te, our choice for the local part and for the maximum angular momentum component ($l^{\rm max}$) of the nonlocal one are $loc = p$ and $l^{\rm max} = d$. This is identical to what is commonly employed in the literature. Instead, for Ge, we made an alternative selection, namely, $loc = p$, $l^{\rm max} = p$. This option features an extended record of reliability for a large variety of disordered chalcogenide materials [40–44].

The initial configuration, common to all simulations, consisted of a disordered system of 144 atoms (32 Ge, 32 Sb, and 80 Te) in a cubic simulation cell of side 16.86 Å, corresponding to a density of 0.030 atom Å^{-3}, on which periodic boundary conditions were applied. NVT simulations were performed at T = 300 (40 ps), 600 (20 ps), 900 (70 ps), 600 (50 ps), and 300 (42 ps) K. The overall features of the network topology (tetrahedral versus octahedral coordination) are not substantially modified when releasing the residual pressure on the initial volume via a slight expansion. Statistics were collected on this last part of the thermal cycle over the last 30 ps. We remark that at 900 K the system shows a high mobility and broad pair correlation functions typical of a liquid state. Given these conditions, atomic displacements covered distances of several atomic bond lengths ensuring effective loss of memory of the initial configuration. Three systems were produced, differing by the XC functional and the type of valence-core PPs. Namely, a first system generated within a BLYP XC functional and TM PPs (BLYP-TM), a second one within a PBE XC functional and TM PPs (PBE-TM), and a third one (BLYP-GTH) within the identical BLYP XC functional of the first case but making use of GTH PPs (BLYP-GTH).

To establish correlations between the structural features of the GST network and its chemical bonding properties, we calculated maximally localized Wannier functions [45,46] averaged over 200 configurations sampled along the last 25 ps. The analysis of the Wannier centers with respect to the nuclear positions proved instrumental in gaining insight into the correlation between structural and bonding properties for several disordered chalcogenides [42,47,48].

III. STRUCTURAL PROPERTIES

A. Total structure factors and pair correlation functions

The neutron and x-ray scattering structure factors of amorphous GST for the BLYP-TM and PBE-TM systems are compared to experimental data in Fig. 1. The intensities of all the peaks are well reproduced with an accuracy of 90% or

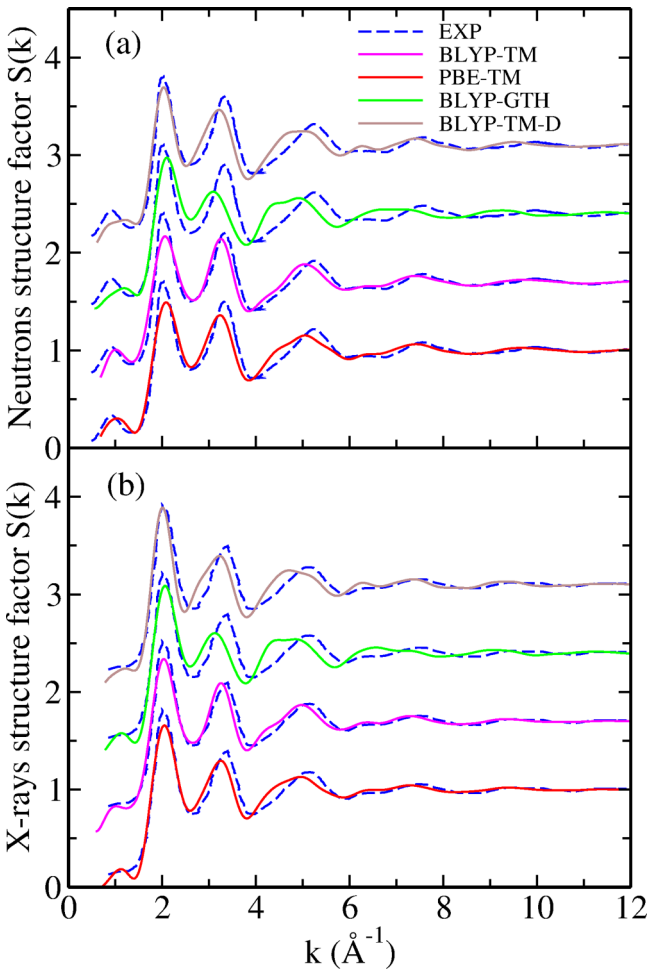

FIG. 1. Calculated and experimental neutrons (a) and x-ray (b) total structure factor $S(k)$ of amorphous $Ge_2Sb_2Te_5$. X-ray and neutrons experimental data are taken from Refs. [26,27], respectively. The BLYP-TM (magenta line), PBE-TM (red line), BLYP-GTH (green line), and BLYP-TM-D (brown line) are compared to experimental data (dashed blue line).

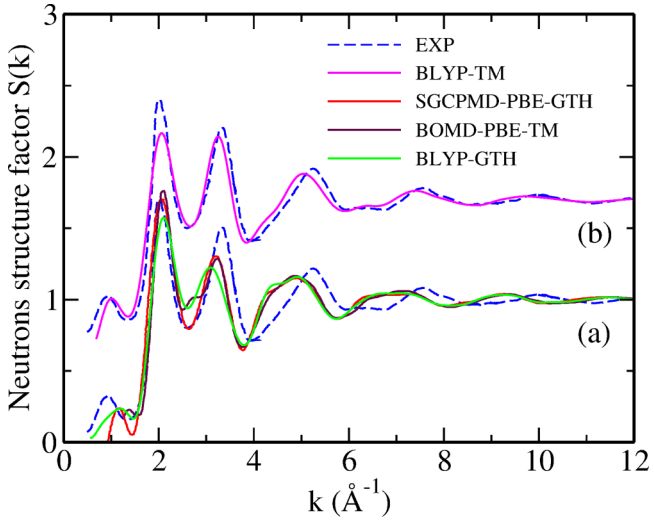

FIG. 2. Calculated and measured total neutrons structure factor $S(k)$ of amorphous $Ge_2Sb_2Te_5$. (a) The BLYP-GTH results (green line), SGCPMD-PBE-GTH simulations from Refs. [19] (red line) and BOMD-PBE-TM simulations from Ref. [18] (maroon line) are compared to experimental data from Ref. [27] (dashed blue line). (b) The BLYP-TM results (magenta line) is compared to experimental data (dashed blue line).

more. The only notable discrepancy is a shift in the position of the third peak around 5 Å^{-1}. Concerning the two XC functionals, BLYP-TM and PBE-TM perform similarly for $k < 4$ Å^{-1}, while in the range 4–9 Å^{-1} PBE-TM deviates slightly from the experimental curve, in contrast with the excellent behavior of BLYP-TM.

The disagreement with experiments is much more severe in the BLYP-GTH case. Knowing that the performance of a given model is at its best for smaller values of the Wright parameter R_χ [49] [Eq. (2)], BLYP-TM features values of R_χ roughly half (R_χ equal to 6.84%) of those found previously by FPMD-DFT models,

$$R_\chi \equiv \left\{ \frac{\sum_i [S_{\rm exp}(k_i) - S_{\rm FPMD}(k_i)]^2}{\sum_i S^2_{\rm exp}(k_i)} \right\}^{1/2}. \qquad (2)$$

Here, $S_{\rm exp}(k_i)$ and $S_{\rm FPMD}(k_i)$ are the experimental and the simulated structure factors at a given wave vector k_i. Worth of note is also the R_χ values for the PBE-TM case, equal to 7.31.

Figure 2 exemplifies the different performances of the DFT schemes employed, by focusing separately on (i) those for which the agreement on the total neutrons structure factor is less satisfactory [Fig. 2(a)] and (ii) on our BLYP-TM results [Fig. 2(b)]. All theoretical models are compared to neutron diffraction measurements from Ref. [27]. The results considered in Fig, 2(a) refer to our BLYP-GTH model and to those of Ref. [18] [Born-Oppenheimer simulation (BOMD) with PBE XC functional and TM PPs, called hereafter BOMD-PBE-TM] and Ref. [19] [second generation Car-Parrinello simulation (SGCPMD) with PBE functional and GTH PPs, called hereafter SGCPMD-PBE-GTH]. We found R_χ equal to 12.93% for BLYP-GTH, to 12.68% for BOMD-PBE-TM, and to 12.09% for SGCPMD-PBE-GTH. The origin of the lower R_χ (6.84%) in the BLYP-TM case [Fig. 2(b)] deserves to be rationalized in detail. In this context, the selection of the exchange-correlation functional cannot be invoked to account for the recorded behaviors, since BLYP-GTH, BOMD-PBE-TM, and SGCPMD-PBE-GTH lead to very close results. Therefore we analyzed the specific pseudopotential constructions adopted in the present and in previous studies.

TABLE I. Maximum angular momentum $l^{\rm max}$ used in the KB construction of pseudopotentials.

	Kleinman-Baylander construction		
Simulation	Ge	Sb	Te
TM this work	$l^{\rm max} = p$	$l^{\rm max} = d$	$l^{\rm max} = d$
TM Ref. [18]	$l^{\rm max} = d$	$l^{\rm max} = d$	$l^{\rm max} = d$
GTH this work	$l^{\rm max} = d$	$l^{\rm max} = d$	$l^{\rm max} = d$
GTH Ref. [19]	$l^{\rm max} = d$	$l^{\rm max} = d$	$l^{\rm max} = d$

In order to understand what makes our Ge TM PP different from other PPs, we looked at the Kleinman-Baylander (KB) construction used in each work. As shown in Table I, we use $l^{\rm max} = p$ as the maximum channel in the KB construction of the Ge PP, while the TM PP from Ref. [18] as well as our GTH and the GTH scheme from Ref. [19] have d as the maximum channel in the Ge PP.

Given these premises, the question arises on the hypothesized impact of this construction on the structural properties of glassy GST. To assess this point, an amorphous GST system has been generated following the same recipe adopted for BLYP-TM and taking the Ge PP with $l^{\rm max} = d$ (this model is called hereafter BLYP-TM-D). The Ge electronic structure is [Ar] $3d^{10}$ $4s^2$ $4p^2$, thus the d channel included in the pseudopotential is empty. Results are compared to experiments and to the BLYP-TM case ($l^{\rm max} = p$) in Fig. 1.

For the BLYP-TM-D case, we find a Wright parameter R_χ equal to 10.95%. This value is similar to the one found with the BLYP-GTH, BOMD-PBE-TM and SGCPMD-PBE-GTH schemes. Overall, it appears that the FPMD performances in the case of glassy GST acquire a stronger quantitative character when adopting $l^{\rm max} = p$ in the Ge PPs. This legitimates the choice adopted throughout the present paper.

Partial pair correlation functions (PCFs) are reported in Fig. 3, while related coordination numbers are listed in Table II. These are determined using as a cutoff distance criterion the first minimum of each $g_{\alpha\beta}(r)$, apart from the Sb–Te bonds, where a cutoff radius of 3.4 Å was selected on the basis of the outer edge of the Sb–Te PCF in the crystal phase. For completeness, a comparison of the partial pair correlation functions obtained via BLYP-TM and BLYP-TM-D is provided in Fig. 4. The first peak in both the Ge-Ge and Ge-Sb PCFs is assigned to the presence of Ge–Ge and Ge–Sb "wrong bonds." Following the terminology of Ref. [51], we define as wrong bonds those that do not occur in the crystal. At variance with former models obtained by typical melt-quench procedures [19,21] our results show a considerable amount of "wrong bonds." In this respect, our results are in line with the estimate obtained on the basis of experimental high energy x-ray and K-edge EXAFS measurements [28]. While the PBE-TM model slightly overestimates bond lengths

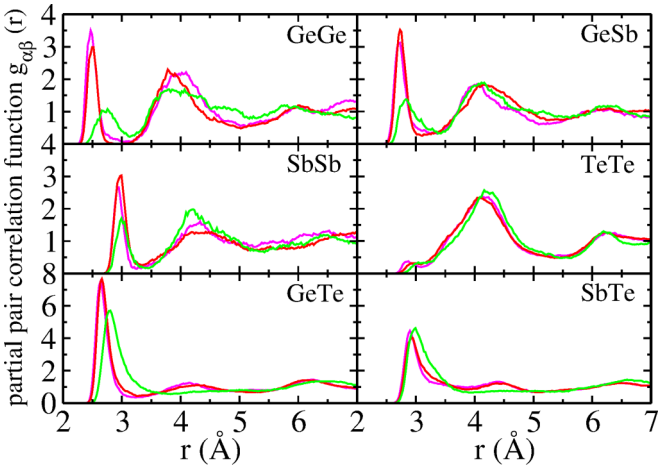

FIG. 3. Partial pair correlation functions of amorphous $Ge_2Sb_2Te_5$ for the BLYP-TM (magenta line), PBE-TM (red line), and BLYP-GTH (green line) models.

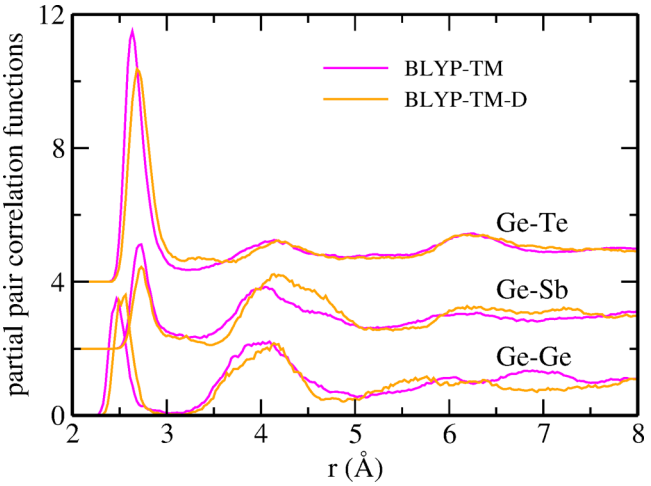

FIG. 4. Partial pair correlation functions Ge-Ge, Ge-Sb, and Ge-Te as obtained from BLYP-TM (magenta line) and BLYP-TM-D (orange line) models.

and coordination numbers, the BLYP-TM one reproduces accurately the r_{GeGe}, r_{GeTe}, and r_{SeTe} distances.

B. Coordination number and analysis of local environment

The distribution of the coordination numbers for Ge, Sb, and Te are shown in Fig. 5. The local environment turns out to be rather similar for both the BLYP-TM and the PBE-TM systems, the difference being less than 5%, whereas significant differences are found for the BLYP-GTH case. Glassy $Ge_2Sb_2Te_5$ exhibits a large amount (∼80%) of fourfold Ge sites. Among these fourfold atoms, Ge-Ge_nTe_{4-n} ($n = 0,1$) are the most abundant, i.e., 38.6% for BLYP-TM and 38.9% for PBE-TM. Sb is mainly threefold (∼60%) with ∼30% of fourfold configurations and Te is mainly twofold (∼60%) with ∼30% of threefold atoms. Such a topology provides a new picture of glassy GST, corresponding to the best agreement recorded so far with experimental data.

Clear cut information on the atomic structure can be obtained from the order parameter [52] $q = 1 - \frac{3}{8}\sum_{i>k}(\frac{1}{3} + \cos\theta_{ijk})^2$. Such parameter is able to quantify the different weight of distinct coordination, the sum running over the bonded atom pairs where j is the central atom forming a bonding angle θ_{ijk} with its neighbors. For a perfect tetrahedron, the order parameter is $q = 1$, while $q = 0$ refers to a sixfold octahedral environment. Defective octahedra correspond to

TABLE II. Bond lengths ($r_{\alpha\beta}$) and partial coordination numbers ($n_{\alpha\beta}$) extracted from the partial pair correlation functions [$g_{\alpha\beta}(r)$] of amorphous $Ge_2Sb_2Te_5$ models generated with BLYP and PBE XC functionals. α and β denote the two atomic species. TGe is the fraction Ge atoms in tetrahedral geometry. Experimental results are from Refs. [9,10]. SGCPMD stands for "second generation Car-Parrinello molecular dynamics," while BOMD stands for "Born-Oppenheimer molecular dynamics." It should be noted that the BLYP-TM results of Ref. [50] were obtained by combining PBE pseudopotentials and BLYP exchange-correlation functionals (private communication by the authors). We have used the following cutoff distances as determined from the first minimum of each $g_{\alpha\beta}(r)$: $r_{\mathrm{GeGe}} = 3.1, 2.9, 3.1$ Å, $r_{\mathrm{GeSb}} = 3.3, 3.2, 3.3$ Å, $r_{\mathrm{GeTe}} = 3.2, 3.3, 3.5$ Å, $r_{\mathrm{SbSb}} = 3.2, 3.3, 3.4$ Å, $r_{\mathrm{SbTe}} = 3.4, 3.4, 3.4$ Å, and $r_{\mathrm{TeTe}} = 3.1, 3.1, 3.2$ Å, for BLYP-TM, PBE-TM, and BLYP-GTH, respectively.

		This work			SGCPMD		BOMD	VASP		
	Exp a:[9], b:[10]	BLYP-TM	PBE-TM	BLYP-GTH	BLYP-GTH [11]	PBE-GTH [19]	PBE-TM [18]	BLYP-TM [50]	PBE-TM [50]	HSE [50]
r_{GeGe}	2.47^b	2.47	2.49	2.75	–	–	–	–	–	–
r_{GeSb}	–	2.73	2.73	2.82	–	–	–	–	–	–
r_{GeTe}	2.61^a, 2.63^b	2.63	2.66	2.8	–	–	2.78	2.74	2.78	2.84
r_{SbSb}	–	2.92	2.99	3.0	–	–	–	–	–	–
r_{SbTe}	2.85^a, 2.83^b	2.89	2.92	3.0	–	–	2.93	2.86	2.93	2.86
n_{GeGe}	0.6 ± 0.2^b	0.42	0.32	0.29	0.29	0.29	–	0.2	0.4	0.6
n_{GeSb}	–	0.59	0.51	0.43	0.29	0.36	–	0.1	0.3	0.4
n_{GeTe}	3.3 ± 0.5^b	3.02	3.30	4.27	3.16	3.31	–	3.0	3.1	2.7
n_{SbSb}	–	0.41	0.56	0.36	0.41	0.43	–	0.4	0.6	0.3
n_{SbTe}	2.8 ± 0.5^b	2.99	3.09	3.85	3.30	3.36	–	2.6	2.3	2.6
n_{TeTe}	–	0.18	0.16	0.20	0.26	0.30	–	0.2	0.4	0.3
TGe (%)	–	68.7	65.7	22.06	33	27	34	42	33	59

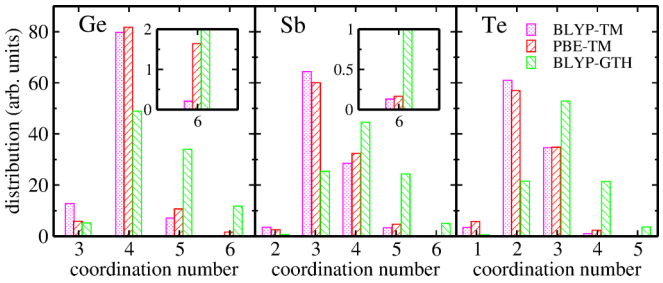

FIG. 5. Fractions of n-fold Ge, Sb, and Te atoms ($n = 1$, 2, 3, 4, 5 or 6) for the BLYP-TM (magenta bar), PBE-TM (red bar), and BLYP-GTH (green bar) models.

$q = 5/8$ for fourfold coordination and $q = 7/8$ for threefold pyramidal ones [17].

Focusing on the BLYP-TM and PBE-TM cases only, the high fraction of fourfold Ge atoms is reflected by the corresponding peak in Fig. 6. This indicates that the majority of fourfold Ge sites has a tetrahedral configuration and the broadening up to $q = 0.5$ is due to defective octahedral fourfold Ge. The fraction of tetrahedral Ge can be estimated by integrating the q ($n_c = 4$) distribution in the range $q = 0.8-1.0$. We obtain 68.7% for BLYP-TM and 65.7% for PBE-TM with the remaining fraction pertaining to defective octahedral configurations. The broad distribution in the range $q = 0$–0.6 for the fivefold Ge is also a signature of defective octahedral configuration.

IV. ELECTRONIC PROPERTIES: NETWORK CHEMICAL BONDING

We seek further insight into the interplay between atomic structure and chemical bonding of GST by resorting to the Wannier formalism, based on the notion of Wannier functions and centers WFC (the W label referring to these degrees of freedom). The WFC formalism provides a powerful tool for an unambiguous characterization of the bond network with respect to the traditional analysis based uniquely on $g_{\alpha\beta}(r)$ [53,54]. Recently, we have employed WFC centers to quantify the different behavior of PBE and BLYP in describing the fingerprints of the bonding and lone pairs subnetworks of glassy $GeTe_4$ [22]. We note that, other methods such as the crystal orbital overlap population method could provide useful insight into the nature of chemical bonds as it was applied in the case of amorphous GeTe [55].

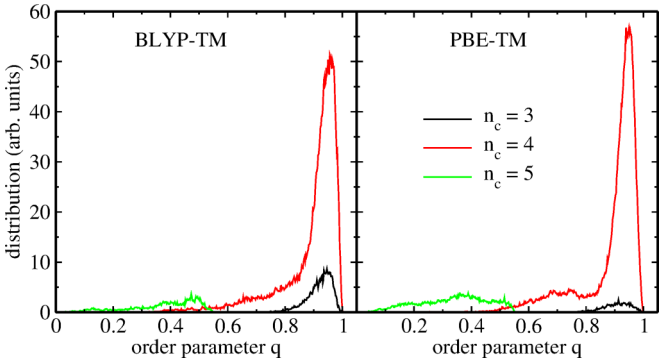

FIG. 6. Distribution of the local order parameter around Ge atom for the BLYP-TM and PBE-TM models. Results are given for different coordination numbers (n_c).

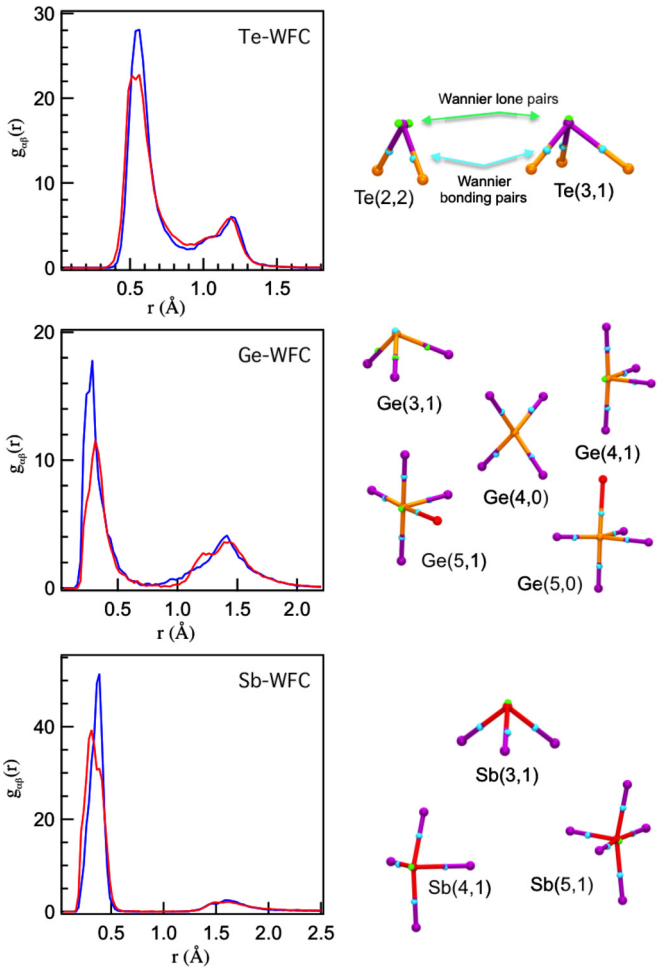

FIG. 7. (Left): Partial pair correlation functions $g_{TeWFC}(r)$ (top), $g_{GeWFC}(r)$ (center), and $g_{SbWFC}(r)$ (bottom). Blue lines refer to BLYP-TM and red lines to PBE-TM data. (Right) Structural units in GST identified with the formalism proposed by Refs. [6,54] based on $M(m,n)$, where M is the central atom (Ge, Sb, Te), m is the nearest-coordinated neighbor, and n is the number of lone pairs. WFC centers corresponding to bonds and lone pairs are depicted by light blue and green spheres, respectively.

In Fig. 7, we compare the pair correlation functions $g_{TeWFC}(r)$, $g_{GeWFC}(r)$, and $g_{SbWFC}(r)$ obtained within the BLYP-TM and PBE-TM frameworks. All three pair correlation functions show two main peaks, corresponding, the first, to the WFC lone pairs [centered at 0.56 Å (Te-WFC), 0.29 Å (Ge-WFC), and 0.39 Å (Sb-WFC)] and the second, to the bonding WFC [centered at 1.19 Å (Te-WFC), 1.42 Å (Ge-WFC), and 1.59 Å (Sb-WFC)]. In the case of glassy $GeTe_4$, BLYP and PBE differed by the presence or absence of a split second peak in $g_{TeWFC}(r)$, denoting homopolar and heteropolar bonding. It appears that such marks are broadened and merged in the case of GST. In view of the very similar BLYP and PBE coordination environments, the main difference between the two XC schemes in terms of correlations with the Wanniers centers is found in the intensity of the peak

corresponding to the WFC lone pairs. This difference simply reflects dissimilar amounts of miscoordinated atoms, at the very origin of the presence of lone pairs. The corresponding units are visualized in the right panels of Fig. 7, according to the formalism proposed in Refs. [6,54]. In the definition of $M(m,n)$, M is the central atom (Ge, Sb, Te), m is the nearest-coordinated neighbor, and n is the number of lone pairs. The above analysis show that the better performances of BLYP in terms of comparison with experimental structural data are not reflected by any striking difference in the electron localization behaviors.

V. CONCLUSIONS

In conclusion, our BLYP-TM model of glassy GST provides a very good account of experimental structural results. We are able to recover realistic values for Ge–Te bonds, corresponding to a combined tetrahedral/octahedral network. Within our model, the tetrahedra are clearly predominant, this conclusion being in agreement with several experimental pieces of evidence and in disagreement with others [5,6,9,10,12,14,15,20]. For instance, it was argued in Ref. [20] that Raman features arising from Ge atoms in tetrahedral coordination are absent in the experimental counterpart, calling for Raman calculations to be performed on the present configurations (see Ref. [56]). Our PBE-TM model is also very well performing, albeit at a slightly lower level in terms of agreement with the pattern of the total structure factor and the interatomic distances. Overall, the bonding features of the two schemes are found to be quite similar, as shown via an analysis of the correlations between the ionic positions and the Wannier centers positions. The predictive power of the BLYP exchange-correlation functional for disordered chalcogenide materials stems from a specific choice of the corresponding Ge PP. It remains true that the debate on the atomic structure of glassy GST awaits further experimental and theoretical contributions, better accounting, as done recently [3,57,58], for structural relaxation and nucleation processes.

ACKNOWLEDGMENT

We acknowledge Pôle HPC Equip@Meso of the University of Strasbourg and GENCI (DARI N. x2016095071) for computer time allocations.

[1] B. Zalba, J. Marín, L. F. Cabeza, and H. Mehling, Appl. Therm. Eng. **23**, 251 (2003).
[2] M. Wuttig and N. Yamada, Nat. Mater. **6**, 824 (2007).
[3] K. V. Mitrofanov, A. V. Kolobov, P. Fons, X. Wang, J. Tominaga, Y. Tamenori, T. Uruga, N. Ciocchini, and D. Ielmini, J. Appl. Phys. **115**, 173501 (2014).
[4] H. S. P. Wong, S. Raoux, S. Kim, J. Liang, J. P. Reifenberg, B. Rajendran, M. Asheghi, and K. E. Goodson, Proc. IEEE **98**, 2201 (2010).
[5] E. Carria, A. M. Mio, S. Gibilisco, M. Miritello, F. d'Acapito, M. G. Grimaldi, and E. Rimini, Electrochem. Solid-State Lett. **14**, H480 (2011).
[6] M. Krbal, A. V. Kolobov, P. Fons, J. Tominaga, S. R. Elliott, J. Hegedus, and T. Uruga, Phys. Rev. B **83**, 054203 (2011).
[7] S. Mukhopadhyay, J. Sun, A. Subedi, T. Siegrist, and D. J. Singh, Sci. Rep. **6**, 25981 (2016).
[8] M. Xu, Y. Q. Cheng, H. W. Sheng, and E. Ma, Phys. Rev. Lett. **103**, 195502 (2009).
[9] A. V. Kolobov, P. Fons, A. I. Frenkel, A. L. Ankudinov, L. Alexei, J. Tominaga, and T. Uruga, Nat. Mater. **3**, 703 (2004).
[10] D. A. Baker, M. A. Paesler, G. Lucovsky, S. C. Agarwal, and P. C. Taylor, Phys. Rev. Lett. **96**, 255501 (2006).
[11] S. Caravati and M. Bernasconi, Phys. Status Solidi B **252**, 260 (2015).
[12] M. A. Paesler, D. A. Baker, G. Lucovsky, A. E. Edwards, and P. C. Taylor, J. Phys. Chem. Solids **68**, 873 (2007).
[13] S. Sen, T. G. Edwards, J.-Y. Cho, and Y. C. Joo, Phys. Rev. Lett. **108**, 195506 (2012).
[14] S. Hosokawa, T. Ozaki, K. Hayashi, N. Happo, M. Fujiwara, K. Horii, P. Fons, A. V. Kolobov, and J. Tominaga, Appl. Phys. Lett. **90**, 131913 (2007).
[15] M. Hada, W. Oba, M. Kuwahara, I. Katayama, T. Saiki, J. Takeda, and K. G. Nakamura, Sci. Rep. **5**, (2015).
[16] W. Wełnic, A. Pamungkas, R. Detemple, C. Steimer, S. Blügel, and M. Wuttig, Nat. Mater. **5**, 56 (2006).
[17] S. Caravati, M. Bernasconi, T. D. Kühne, M. Krack, and M. Parrinello, App. Phys. Lett. **91**, 171906 (2007).
[18] J. Akola and R. O. Jones, Phys. Rev. B **76**, 235201 (2007).
[19] S. Caravati, M. Bernasconi, T. D. Kühne, M. Krack, and M. Parrinello, J. Phys.: Condens. Matter. **21**, 255501 (2009).
[20] G. C. Sosso, S. Caravati, R. Mazzarello, and M. Bernasconi, Phys. Rev. B **83**, 134201 (2011).
[21] J. Akola, J. Larrucea, and R. O. Jones, European Phase-Change and Ovonics Symposium **128** (2010), https://docs.wixstatic.com/ugd/3d44dd_0a7e89a4dc704a4dac2830579d32dc6a.pdf.
[22] A. Bouzid, C. Massobrio, M. Boero, G. Ori, K. Sykina, and E. Furet, Phys. Rev. B **92**, 134208 (2015).
[23] A. D. Becke, Phys. Rev. A **38**, 3098 (1988).
[24] C. Lee, W. Yang, and R. G. Parr, Phys. Rev. B **37**, 785 (1988).
[25] N. Troullier and J. L. Martins, Phys. Rev. B **43**, 1993 (1991).
[26] S. Kohara, K. Kato, S. Kimura, H. Tanaka, T. Hitoshi, T. Usuki, K. Suzuya, H. Tanak, Y. Moritomo, T. Matsunaga, N. Yamada, Y. Tanaka, H. Suematsu, and M. Takata, Appl. Phys. Lett. **89**, 201910 (2006).
[27] P. Jóvári, I. Kaban, J. Steiner, B. Beuneu, A. Schöps, and M. A. Webb, Phys. Rev. B **77**, 035202 (2008).
[28] P. Jóvári, I. Kaban, J. Steiner, B. Beuneu, A. Schöps, and A. Webb, J. Phys.: Condens. Matter **19**, 335212 (2007).
[29] R. Car and M. Parrinello, Phys. Rev. Lett. **55**, 2471 (1985).
[30] CPMD, http://www.cpmd.org/, Copyright IBM Corp 1990-2013, Copyright MPI für Festkörperforschung Stuttgart, 1997-2001.
[31] J. P. Perdew, K. Burke, and M. Ernzerhof, Phys. Rev. Lett. **77**, 3865 (1996).
[32] S. Goedecker, M. Teter, and J. Hutter, Phys. Rev. B **54**, 1703 (1996).
[33] M. Krack, Theor. Chem. Acc. **114**, 145 (2005).
[34] S. Nosé, Mol. Phys. **52**, 255 (1984).
[35] S. Nosé, J. Chem. Phys. **81**, 511 (1984).
[36] W. G. Hoover, Phys. Rev. A **31**, 1695 (1985).

[37] G. J. Martyna, M. L. Klein, and M. Tuckerman, J. Chem. Phys. **97**, 2635 (1992).

[38] P. E. Blöchl and M. Parrinello, Phys. Rev. B **45**, 9413 (1992).

[39] L. Kleinman and D. M. Bylander, Phys. Rev. Lett. **48**, 1425 (1982).

[40] S. Le Roux, A. Bouzid, K. Y. Kim, S. Han, A. Zeidler, P. S. Salmon, and C. Massobrio, J. Chem. Phys. **145**, 084502 (2016).

[41] A. Bouzid, S. Le Roux, G. Ori, M. Boero, and C. Massobrio, J. Chem. Phys. **143**, 034504 (2015).

[42] A. Bouzid, K. J. Pizzey, A. Zeidler, G. Ori, M. Boero, C. Massobrio, S. Klotz, H. E. Fischer, C. L. Bull, and P. S. Salmon, Phys. Rev. B **93**, 014202 (2016).

[43] K. Wezka, A. Bouzid, K. J. Pizzey, P. S. Salmon, A. Zeidler, S. Klotz, H. E. Fischer, C. L. Bull, M. G. Tucker, M. Boero, S. Le Roux, C. Tugène, and C. Massobrio, Phys. Rev. B **90**, 054206 (2014).

[44] S. Le Roux, A. Bouzid, M. Boero, and C. Massobrio, Phys. Rev. B **86**, 224201 (2012).

[45] R. Resta and S. Sorella, Phys. Rev. Lett. **82**, 370 (1999).

[46] N. Marzari and D. Vanderbilt, Phys. Rev. B **56**, 12847 (1997).

[47] G. Ori, C. Massobrio, A. Bouzid, M. Boero, and B. Coasne, Phys. Rev. B **90**, 045423 (2014).

[48] A. Bouzid and A. Pasquarello, Phys. Rev. Appl. **8**, 014010 (2017).

[49] A. C. Wright, R. N. Sinclair, and A. J. Leadbetter, J. Non-Cryst. Solids **71**, 295 (1985).

[50] K. Y. Kim, D.-Y. Cho, B. Cheong, D. Kim, H. Horii, and S. Han, J. Appl. Phys. **113**, 134302 (2013).

[51] J. Akola and R. O. Jones, J. Phys.: Condens. Matter **20**, 465103 (2008).

[52] J. R. Errington and P. G. Debenedetti, Nature (London) **409**, 318 (2001).

[53] F. Zipoli, D. Krebs, and A. Curioni, Phys. Rev. B **93**, 115201 (2016).

[54] T. H. Lee and S. R. Elliott, Adv. Mater. **29**, 1700814 (2017).

[55] V. L. Deringer, W. Zhang, M. Lumeij, S. Maintz, M. Wuttig, R. Mazzarello, and R. Dronskowski, Angew. Chem. Int. Ed **53**, 10817 (2014).

[56] See Supplemental Material at http://link.aps.org/supplemental/10.1103/PhysRevB.96.224204 for 100 configurations sampling the trajectory of the BLYP-TM model at $T = 300$ K.

[57] J. Y. Raty, W. Zhang, J. Luckas, C. Chen, R. Mazzarello, C. Bichara, and M. Wuttig, Nat. Commun. **6**, 7467 (2015).

[58] I. Ronneberger, W. Zhang, H. Eshet, and R. Mazzarello, Adv. Funct. Mater. **25**, 6407 (2015).